Proceedings of CONF-FMCE 2026 Symposium: Smart City and Infrastructure Engineering
DOI: 10.54254/2755-2721/2026.CH36688

Boundary-Condition Fidelity and Reynolds-Number Effects in CFD Validation for Vehicle Aerodynamics

Yufan Niu

The Experimental High School Attached to Beijing Normal University, Beijing, China
yufan_080712@outlook.com

Abstract. Credible validation of computational fluid dynamics (CFD) in vehicle aerodynamics depends on the engineering decision being supported. For a fixed vehicle at one operating condition, total drag with quantified uncertainty may be sufficient when only that force is required. It is insufficient, however, for explaining a flow mechanism, predicting a design delta, ranking closely spaced concepts, or transferring a model across geometries and conditions. Starting from the nondimensional governing equations, this paper examines three linked causes: geometric scaling changes Reynolds number and relative boundary-layer thickness; ground, wheel, and tunnel treatments change the represented physical system; and local errors may cancel in an integrated force. Evidence from Ahmed-body, detailed-vehicle, wind-tunnel, moving-ground, and rotating-wheel studies is evaluated through comparison. A decision-oriented framework then separates numerical verification from physical validation and links the required evidence to the intended use. Vehicle CFD is best treated as a conditional prediction whose credibility is bounded by geometry, operating state, physical setup, quantity of interest, and decision.

Keywords: Vehicle aerodynamics, CFD validation, Reynolds number, boundary conditions, uncertainty

1. Introduction

CFD does not predict the aerodynamics of geometry alone. It solves a mathematical model for a specified fluid, domain, operating state, and set of initial and boundary conditions. An open-road simulation and a wind-tunnel test can therefore represent different physical systems even when their nominal vehicle geometry is identical. The test includes finite blockage, supports, a tunnel pressure gradient, a floor boundary layer, and a particular road-simulation system.

Validation is a comparison for stated quantities and conditions, with numerical and experimental uncertainties distinguished from model-form error [1]. Yet vehicle studies are still commonly judged by agreement in total drag. This paper asks how Reynolds-number mismatch, ground and wheel treatment, wind-tunnel representation, and numerical assumptions affect what can validly be inferred from vehicle CFD. It develops a physics-based framework and evaluates its implications through comparison with benchmark and detailed-vehicle literature.

The argument is decision-dependent. Agreement in a global force may provide sufficient validation evidence for a fixed-geometry, fixed-condition task if its combined uncertainty is small

© 2026 The Authors. This is an open access article distributed under the terms of the Creative Commons Attribution License 4.0 (https://creativecommons.org/licenses/by/4.0/).

enough for the decision. It cannot by itself establish local causality, the effect of a small design change, or predictive validity beyond that state. Baseline agreement may arise from component-error cancellation, yet the same model may fail to predict the sign or ranking of a later design delta. Geometry and state, similarity, physical boundary conditions, numerics, and observables must be examined as connected evidence; not every calculation requires maximum fidelity.

2. Literature selection and analytical method

Sources were identified through targeted benchmark searches and citation chaining around the Ahmed body [2] and the principal validation mechanisms. Available full texts were coded by geometry, scale, method, setup, numerics, observable, result, and limitation. Metadata were checked against publisher or proceedings records; unverified copies were excluded from substantive claims. This was not a systematic review.

Differences in geometry, length scale, facility, closure, and error definition preclude a universal discrepancy percentage. Numerical values are therefore treated as case-specific evidence, not transferable correction factors.

Each discrepancy is classified by physical state, numerics, measurement, or interaction, then checked against integrated and local-flow evidence. This prevents a close drag value from outweighing contradictory pressure or wake data.

3. Theoretical framework

3.1 Governing equations and closure

For low-speed external vehicle flow, the nondimensional incompressible equations are

$$\nabla^* \cdot \mathbf{u}^* = 0, \frac{\partial \mathbf{u}^*}{\partial t^*} + \mathbf{u}^* \cdot \nabla^* \mathbf{u}^* = -\nabla^* p^* + \frac{1}{\mathrm{Re}} \nabla^{*2} \mathbf{u}^*, \mathrm{Re} = \frac{\rho U L}{\mu} \tag{1}$$

Equation (1) shows that geometric similarity alone is insufficient: dynamic similarity also requires the relevant dimensionless parameters and boundary conditions to match. Engineering vehicle CFD usually solves Reynolds-averaged or scale-resolving equations. Reynolds averaging introduces the additional stress shown in Eq. (2):

$$\rho\left(\frac{\partial \overline{u_i}}{\partial t} + \overline{u_j}\frac{\partial \overline{u_i}}{\partial x_j}\right) = -\frac{\partial \overline{p}}{\partial x_i} + \mu \nabla^2 \overline{u_i} - \frac{\partial\left(\rho \overline{u_i' u_j'}\right)}{\partial x_j} \tag{2}$$

The new stress must be modelled or partially resolved. Turbulence closure, wall treatment, grid, time step, and averaging duration therefore form part of the prediction, especially when separation and reattachment are sensitive. Krajnovic and Davidson's Ahmed-body LES [3] and Guilmineau's comparison of six URANS closures [4] illustrate that agreement in one separation regime does not establish model validity in another.

3.2 Similarity constraints

A useful validation state is not one Reynolds number but a schematic, non-exhaustive vector,

DOI: 10.54254/2755-2721/2026.CH36688

$$\mathbf{\Pi}_{\text{state}} \approx \left\{\mathrm{Re}_L, \left\{\mathrm{Re}_i\right\}, \mathrm{Ma}, \lambda, \frac{h}{L}, \frac{k_s}{L}, \beta, \frac{U(y,z)}{U_{\text{ref}}}, \mathrm{Tu}, \frac{L_t}{L}, \frac{\Omega R}{U}, \alpha, \ldots\right\} \tag{3}$$

Where Re_i denotes component Reynolds numbers, h/L ground clearance, k_s/L relative roughness, β blockage, $U(y,z)/U_{ref}$ the normalized inlet profile, Tu turbulence intensity, L_t/L normalized turbulence length scale, Ω R/U wheel-speed ratio, and α the yaw angle. The entries relevant to a particular study depend on its geometry and quantity of interest. If a geometrically similar model has scale $\lambda=L_m/L_f$ and uses the same fluid at approximately the same thermodynamic state.

$$\frac{\mathrm{Re}_m}{\mathrm{Re}_f} = \lambda \frac{U_m}{U_f}, \frac{\mathrm{Ma}_m}{\mathrm{Ma}_f} = \frac{U_m}{U_f} \tag{4}$$

At equal speed, $\mathrm{Re}_m/\mathrm{Re}_f=\lambda$. Matching Reynolds number instead requires $U_m/U_f=1/\lambda$, which raises Mach number by the same factor. A strongly reduced model may therefore be unable to match both Reynolds and low-Mach conditions.

Scale also acts locally. For an idealized smooth, zero-pressure-gradient flat plate, order-of-magnitude estimates give $\delta_{99}/x\approx5\mathrm{Re}_x^{-1/2}$ for laminar flow and approximately $0.37\mathrm{Re}_x^{-1/5}$ for turbulent flow [5]. These relations do not predict the actual underbody boundary layer of a vehicle, where pressure gradients, curvature, transition, wheel wakes, and separation are important. They show only the direction and approximate scale of a Reynolds-number effect. Taking x to be of order L gives the scaling used below.

$$\frac{\delta}{h} = \frac{\frac{\delta}{L}}{\frac{h}{L}} \tag{5}$$

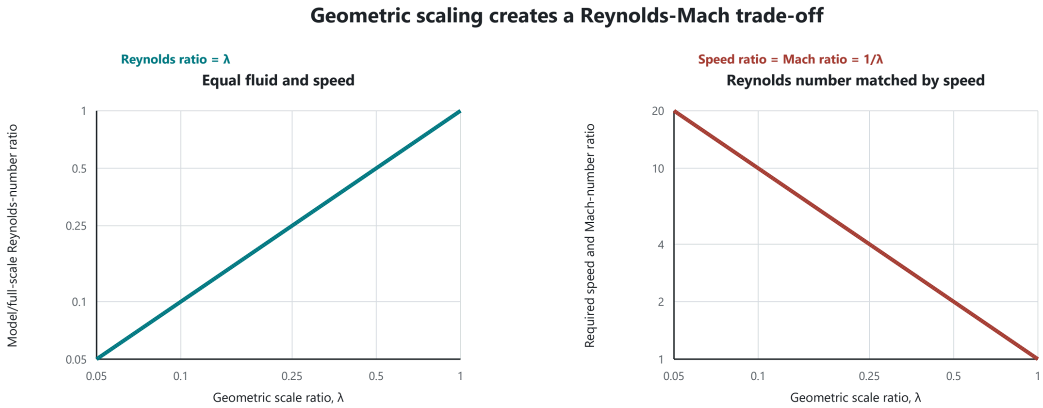

Figure 1. Consequences of model scale λ in the same fluid. Equal speed reduces Reynolds number in direct proportion to scale; matching Reynolds number requires inverse speed and Mach-number ratios. Curves are analytical relations from Eq. (4), not experimental data

Lower Reynolds number can make a boundary layer occupy more of an underbody gap even when geometry is scaled exactly. Edge radius, tyre grooves, roughness, gaps, and manufacturing deviations likewise become larger relative to local dimensions. Transferability depends on whether scaling changes transition, separation, reattachment, or component interaction, rather than on a vehicle-length Reynolds number alone. The location dependence is explicit in the benchmark evidence: a sharp rear edge fixed separation, whereas the upstream roof boundary layer and the 25-

DOI: 10.54254/2755-2721/2026.CH36688

degree slant reattachment remained sensitive to Reynolds number and closure [3, 4]. The coupled Reynolds-Mach consequences of geometric scaling are shown in Figure 1.

3.3 Observables, cancellation, and uncertainty

Local pressure and wall shear are represented by:

$$C_p = \frac{p-p_{\text{ref}}}{\frac{1}{2}\rho {U_{\text{ref}}}^2}, C_f = \frac{\tau_w}{\frac{1}{2}\rho {U_{\text{ref}}}^2} \tag{6}$$

while total drag is their surface projection.

$$C_D = \frac{1}{A_{\text{ref}}} \int_S [-C_p n_x + C_f t_x] \mathrm{d}S = \sum C_{D,i} \tag{7}$$

Opposite component errors can cancel in Eq. (7), so a correct C_D does not prove correct pressure, shear, wake, or lift balance. Reference quantities can add another error. The signed first-order logarithmic differential is:

$$\frac{\mathrm{d}C_D}{C_D} \approx \frac{\mathrm{d}D}{D} - \frac{\mathrm{d}\rho}{\rho} - 2\frac{\mathrm{d}U_{\text{ref}}}{U_{\text{ref}}} - \frac{\mathrm{d}A_{\text{ref}}}{A_{\text{ref}}} \tag{8}$$

so a +1% speed-reference perturbation produces approximately a -2% change in the reported coefficient if force and the other references are unchanged. Equation (8) is a local sensitivity relation, not a root-sum-square estimate of statistical uncertainty; an uncertainty budget would require distributions, correlations, and a stated propagation method.

Numerical verification must precede physical interpretation. For three systematically refined grids, the observed order p can be estimated from solution differences; a fine-grid convergence index is then reported in the form.

$$\text{GCI}_{\text{fine}} = F_s \frac{\left|\frac{Q_2-Q_1}{Q_1}\right|}{r^p-1} \tag{9}$$

Where r is refinement ratio and F_s a safety factor [6]. Non-monotonic convergence requires investigation rather than forced use of Eq. (9). Verification asks whether the selected equations were solved accurately; validation asks whether those equations and inputs represent the intended physical system [1]. For interpretation, an observed residual may be represented schematically as:

$$Q_{\text{CFD}}(\mathbf{x}_s) - Q_{\text{exp}}(\mathbf{x}_e) \approx \varepsilon_{\text{num}} + \varepsilon_{\text{model}} + \Delta Q_{\text{setup}} + \varepsilon_{\text{meas}} + \varepsilon_{\text{int}} \tag{10}$$

Here ΔQ_{setup} is the physical consequence of different states, while ε_{int} acknowledges interactions. The terms need not be independent, additive, or identifiable from one residual. For small differences only, ΔQ_{setup} may be linearized as $\nabla_x Q \cdot (x_s - x_e)$; regime changes require direct sensitivity studies. A wheel-speed mismatch may weakly affect total drag yet strongly affect wheel-wake velocity. Validation should report the mismatch and, where established, the sensitivity of the decision-relevant observable. The coupled pathways are summarized in Figure 2.

DOI: 10.54254/2755-2721/2026.CH36688

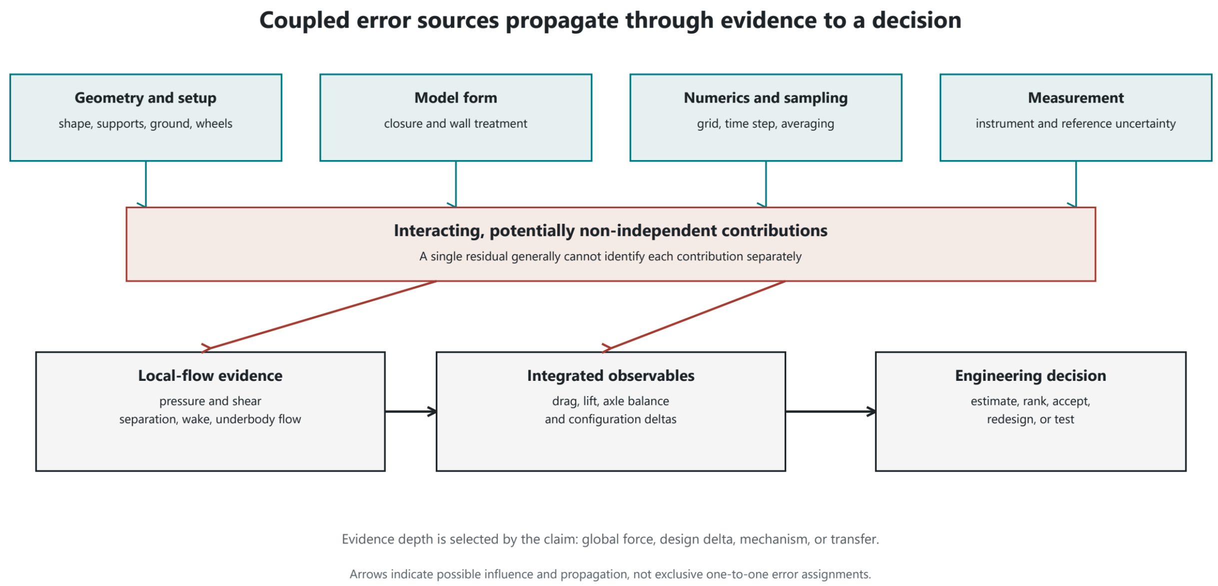

Figure 2. Coupled validation framework. Error sources can interact and can affect both local-flow evidence and integrated observables; arrows indicate possible propagation, not an exclusive one-to-one assignment. The required evidence is set by the engineering decision

4. Evidence across vehicle-aerodynamics studies

4.1 Reynolds number and geometry

Krajnovic and Davidson [3] simulated a 25-degree Ahmed body at height-based $Re=2.0\times10^5$, against experiments at 7.68×10^5. Many post-separation wake quantities agreed because the sharp rear edge fixed separation, although roof boundary-layer differences persisted. That result does not transfer automatically to smooth separation. Guilmineau [4] found that several closures represented the broadly separated 35-degree case, while none captured the measured separation and reattachment at 25 degrees. For three one-third-scale MIRA bodies, Wang et al. [7] observed limited drag variation above a wheelbase Reynolds number of about 1.48×10^6, but this is a configuration-specific plateau, not a universal threshold. Together, these studies support the theoretical criterion: Reynolds mismatch matters most when it changes the governing local flow mechanism.

4.2 Tunnel, ground, and wheel fidelity

Facility representation can change the validation target. Fischer et al. [8] found raw drag spreads of 27-39 counts across model and tunnel setups; selected corrections reduced experimental spread to about one count but did not resolve lift errors. Cyr et al. [9] similarly showed that scanned geometry, road simulation, and reference corrections formed one coupled chain.

The same vehicle can also produce different results in different facilities. Collin et al. [10] measured DrivAer drag differences of about 0.007-0.008 and a front-lift difference near 0.024 between two open-jet tunnels; local $|\Delta C_p|$ exceeded 0.01 even where drag interference nearly cancelled. Thus low blockage or corrected drag alone cannot establish local equivalence.

Ground and wheel labels are also too coarse. Hobeika and Sebben [11] found that a rotating-wall model imposed incorrect kinematics on tyre-groove faces; a groove-aware method improved drag-delta prediction by 0.020 for one covered-rim case while an absolute offset remained. Yamashita et

DOI: 10.54254/2755-2721/2026.CH36688

al. [12] found that moving ground and rotating wheels changed C_D by -0.011 for one two-box underfloor and +0.008 for another. The sign reversal shows that boundary-condition effects are geometry-dependent interactions, not additive corrections.

Complete tunnel modelling can improve selected outputs without validating all outputs. Ljungskog et al. [13] found that, for a production sedan, complete tunnel CFD matched absolute drag within 0.005, while open-road CFD was 0.009-0.014 low; lift and some underbody deltas nevertheless remained incorrect. Higher facility fidelity reduced one error source but did not eliminate geometry, road-system, closure, or numerical error.

Across these cases, facility geometry changes the reference flow, wheel and ground treatments alter near-body kinematics, and corrections can improve drag while leaving lift or local pressure incorrect. Setup fidelity must therefore be judged against the target observable rather than treated as a universal correction.

4.3 Decision-dependent sufficiency of drag agreement

Modern high-resolution datasets clarify where a global metric succeeds and fails. AhmedML [14] produced non-monotonic grid values C_D=0.303, 0.293, 0.285, 0.280 against an experimental 0.299; a selected grid was close globally while local velocity comparison still exposed a missing separation feature. DrivAerML [15] used about 160 million cells per geometry and a statistical stopping criterion, yet retained force offsets and predicted the sign of one total-lift delta incorrectly. High cell count and coefficient agreement are useful evidence, but their sufficiency depends on the claim.

Three uses should be separated. For the total drag of one fixed vehicle and condition, agreement in C_D within stated numerical and experimental uncertainty may suffice. Such agreement does not validate the local flow, although local-flow evidence is unnecessary when the claim is strictly limited to that global force. A design-delta or ranking claim requires stability under plausible changes in grid, boundary conditions, sampling, and model form. A causal or transferable claim requires evidence for the controlling mechanism, such as pressure, separation, wheel wake, or underbody velocity. Constant drag bias may preserve a ranking, whereas an accurate baseline can still give the wrong delta sign. Acceptance criteria should be set before examining the result.

5. Decision-oriented validation framework

The synthesis yields the proposed evidence checklist shown in Table 1. The decision and quantities of interest are defined first. A state audit records geometry, supports, wheel details, roughness, global and component Reynolds numbers, blockage, road simulation, inlet conditions, yaw, and references. Grid, time-step, convergence, and averaging studies address numerical verification. Physical validation selects observables able to challenge the claim. Residuals are traced spatially or by component when a local mechanism or small delta controls the decision, and the validated domain is stated explicitly.

Table 1. Proposed evidence checklist for a bounded validation claim

Evidence area	Evidence to report	Risk if omitted
Geometry/state	Ratios, gaps, supports, roughness, wheel details	Nominally identical models represent different shapes
Similarity	Global and component Re, Ma, blockage, wheel-speed ratio	Scale or operating changes alter the flow regime

Table 1. (continued)

Physical setup	Tunnel, inlet, floor, wheels, yaw, references	CFD and experiment represent different physical systems
Numerics	Grid/time-step study, wall treatment, convergence, averaging	Numerical uncertainty is mistaken for physics
Observables	Decision-selected forces, deltas, pressure, or local flow with uncertainty	Cancellation or wrong sensitivity goes undetected

This framework does not require maximum fidelity or every local observable for every concept calculation. A simplified model is useful for screening if sensitivity tests show that omitted physics does not change the relevant ranking or decision. Additional fidelity and local evidence become necessary when uncertainty overlaps a design delta, when the sign or ranking is unstable, or when the claim concerns a local mechanism or transfer to a new state.

6. Scope and limitations

This study is analytical and literature-based. It does not introduce new simulations, experiments, or a universal numerical correction. The cited cases span different geometries and facilities, so their drag counts, Reynolds thresholds, and sensitivity magnitudes should not be transferred directly between vehicles. AhmedML and DrivAerML are cited as arXiv preprints. These datasets provide transparent methodological cases, not substitutes for independent experimental validation. The proposed framework should be tested prospectively on a defined vehicle and facility before being treated as a complete engineering protocol.

7. Conclusion

Vehicle CFD predicts a represented system, not geometry in isolation. The governing equations show that scale reduction changes Reynolds number and relative boundary-layer thickness unless other parameters are adjusted, while turbulence closure and discretization introduce separate uncertainties. Force integration and reference-speed sensitivity explain why total drag can agree through cancellation even when local physics is wrong.

The reviewed evidence supports a decision-oriented framework covering geometry and state, similarity, physical boundary conditions, numerical treatment, and observables. For a fixed-condition force task, a global coefficient can be sufficient when its uncertainty resolves the decision. Design-change, mechanistic, and transfer claims demand stronger sensitivity and local-flow evidence because baseline agreement can conceal cancellation and cannot guarantee the sign or ranking of a delta. A prediction should be accepted only for the geometry family, operating range, boundary conditions, quantity of interest, and engineering decision for which its evidence has been demonstrated.

References

[1] ASME. (2009). *Standard for verification and validation in computational fluid dynamics and heat transfer* (ASME V&V 20-2009).

[2] Ahmed, S. R., Ramm, G., & Faltin, G. (1984). Some salient features of the time-averaged ground vehicle wake. *SAE Technical Paper 840300*. https://doi.org/10.4271/840300

[3] Krajnovic, S., & Davidson, L. (2005). Flow around a simplified car, Part 1: Large eddy simulation. *J. Fluids Eng., 127*(5), 907-918. https://doi.org/10.1115/1.1989371

DOI: 10.54254/2755-2721/2026.CH36688

[4] Guilmineau, E. (2008). Computational study of flow around a simplified car body. *J. Wind Eng. Ind. Aerodyn., 96*(6), 1207-1217. https://doi.org/10.1016/j.jweia.2007.06.041

[5] Schlichting, H., & Gersten, K. (2017). *Boundary-layer theory* (9th ed.). Springer. https://doi.org/10.1007/978-3-662-52919-5

[6] Celik, I. B., Ghia, U., Roache, P. J., Freitas, C. J., Coleman, H., & Raad, P. E. (2008). Procedure for estimation and reporting of uncertainty due to discretization in CFD applications. *J. Fluids Eng., 130*, 078001. https://doi.org/10.1115/1.2960953.

[7] Wang, Y., Xin, Y., Gu, Z., Wang, S., Deng, Y., & Yang, X. (2014). Numerical and experimental investigations on the aerodynamic characteristic of three typical passenger vehicles. *J. Appl. Fluid Mech., 7*, 659-671. https://doi.org/10.36884/jafm.7.04.21460.

[8] Fischer, O., Kuthada, T., Mercker, E., Wiedemann, J., & Duncan, B. (2010). CFD approach to evaluate wind-tunnel and model setup effects on aerodynamic drag and lift for detailed vehicles. *SAE Technical Paper 2010-01-0760*. https://doi.org/10.4271/2010-01-0760.

[9] Cyr, S., Ih, K.-D., & Park, S.-H. (2011). Accurate reproduction of wind-tunnel results with CFD. *SAE Technical Paper 2011-01-0158*. https://doi.org/10.4271/2011-01-0158.

[10] Collin, C., Mack, S., Indinger, T., & Mueller, J. (2016). A numerical and experimental evaluation of open jet wind tunnel interferences using the DrivAer reference model. *SAE Int. J. Passeng. Cars Mech. Syst., 9*, 657-679. https://doi.org/10.4271/2016-01-1597.

[11] Hobeika, T., & Sebben, S. (2018). CFD investigation on wheel rotation modelling. *Journal of Wind Engineering and Industrial Aerodynamics, 174*, 241-251. https://doi.org/10.1016/j.jweia.2018.01.005.

[12] Yamashita, T., Makihara, T., Saito, Y., Kato, C., Takayama, R., Takayama, T., & Yamade, Y. (2018). Effects of moving ground and rotating wheels on aerodynamic drag of a two-box vehicle. *SAE International Journal of Passenger Cars - Mechanical Systems, 11*, 415-428. https://doi.org/10.4271/2018-01-0730.

[13] Ljungskog, E., Sebben, S., & Broniewicz, A. (2020). Inclusion of the physical wind tunnel in vehicle CFD simulations for improved prediction quality. *Journal of Wind Engineering and Industrial Aerodynamics, 197*, 104055. https://doi.org/10.1016/j.jweia.2019.104055.

[14] Ashton, N., Maddix, D. C., Gundry, S., & Shabestari, P. M. (2024). AhmedML: High-fidelity computational fluid dynamics dataset for incompressible, low-speed bluff body aerodynamics. *arXiv preprint arXiv:2407.20801*. https://doi.org/10.48550/arXiv.2407.20801.

[15] Ashton, N., Mockett, C., Fuchs, M., et al. (2024). DrivAerML: High-fidelity computational fluid dynamics dataset for road-car external aerodynamics. *arXiv preprint arXiv:2408.11969*. https://doi.org/10.48550/arXiv.2408.11969.